Journal of Biomechanics 46 (2013) 2356–2362

Contents lists available at ScienceDirect

Journal of Biomechanics

journal homepage: www.elsevier.com/locate/jbiomech
www.JBiomech.com

# A novel approach to estimate trabecular bone anisotropy using a database approach

Javad Hazrati Marangalou [a], Keita Ito [a], Matteo Cataldi [b], Fulvia Taddei [b], Bert van Rietbergen [a,*]

[a] Orthopaedic Biomechanics, Department of Biomedical Engineering, Eindhoven University of Technology, Eindhoven, The Netherlands
[b] Laboratorio di Tecnologia Medica, Istituti Ortopedici Rizzoli, Bologna, Italy

ARTICLE INFO

*Article history:*
Accepted 31 July 2013

*Keywords:*
Bone
Anisotropy
Database approach
Finite element method

ABSTRACT

Continuum finite element (FE) models of bones have become a standard pre-clinical tool to estimate bone strength. These models are usually based on clinical CT scans and material properties assigned are chosen as isotropic based only on the density distribution. It has been shown, however, that trabecular bone elastic behavior is best described as orthotropic. Unfortunately, the use of orthotropic models in FE analysis derived from CT scans is hampered by the fact that the measurement of a trabecular orientation (fabric) is not possible from clinical CT images due to the low resolution of such images. In this study, we explore the concept of using a database (DB) of high-resolution bone models to derive the fabric information that is missing in clinical images. The goal of this study was to investigate if models with fabric derived from a relatively small database can already produce more accurate results than isotropic models.

A DB of 33 human proximal femurs was generated from micro-CT scans with a nominal isotropic resolution of 82 μm. Continuum FE models were generated from the images using a pre-defined mesh template in combination with an iso-anatomic mesh morphing tool. Each element within the mesh template is at a specific anatomical location. For each element within the cancellous bone, a spherical region around the element centroid with a radius of 2 mm was defined. Bone volume fraction and the mean-intercept-length fabric tensor were analyzed for that region. Ten femurs were used as test cases. For each test femur, four different models were generated: (1) an orthotropic model based on micro-CT fabric measurements (gold standard), (2) an orthotropic model based on the fabric derived from the best-matched database model, (3) an isotropic-I model in which the fabric tensor was set to the identity tensor, and (4) a second isotropic-II model with its total bone stiffness fitted to the gold standard. An elastic-plastic damage model was used to simulate failure and post failure behavior during a fall to the side.

The results show that all models produce a similar stress distribution. However, compared to the gold standard, both isotropic-I and II models underestimated the stress/damage distributions significantly. We found no significant difference between DB-derived and gold standard models. Compared to the gold standard, the isotropic-I models further underestimated whole bone stiffness by 26.3% and ultimate load by 14.5%, while these differences for the DB-derived orthotropic models were only 4.9% and 3.1% respectively.

The results indicate that the concept of using a DB to estimate patient-specific anisotropic material properties can considerably improve the results. We expect that this approach can lead to more accurate results in particular for cases where bone anisotropy plays an important role, such as in osteoporotic patients and around implants.



## 1. Introduction

Patient specific continuum finite element (FE) models have become a standard pre-clinical tool to study mechanical behavior of bone alone or with implants. Such models usually implement material properties with elastic and strength properties that are based on the local bone density as quantified by Hounsfield units in clinical CT images (Keyak, 2001; Liebschner et al., 2003; Taddei et al., 2007; Yosibash et al., 2007). Empirical power–law relationships are then used to derive the elastic and strength properties (Carter and Hayes, 1977; Helgason et al., 2008; Keller, 1994; Lotz et al., 1991; Wirtz et al., 2000; Zannoni et al., 1999). In virtually all studies done so far, material properties assigned to the bone elements are chosen

* Correspondence to: Eindhoven University of Technology, Department of Biomedical Engineering, PO Box 513, GEM-Z 4.118, 5600 MB Eindhoven, The Netherlands. Tel.: +31 40 247 4773; fax: +31 40 247 3744.
*E-mail address:* B.v.Rietbergen@tue.nl (B. van Rietbergen).

0021-9290/$ - see front matter © 2013 Elsevier Ltd. All rights reserved.
http://dx.doi.org/10.1016/j.jbiomech.2013.07.042

as isotropic based on bone density distribution only. Experimental and computational studies, however, have shown that bone can be highly anisotropic, particularly in cancellous bone regions, and that its elastic behavior is best described as orthotropic. In most cases, the experimentally derived power–law relationships are determined only after aligning the measurement direction with the anatomical direction. As such these power–laws may well represent the stiffness and strength in the principal load carrying direction, but will likely overestimate these values in other directions. It was demonstrated that models that account for this anisotropic behavior better predict whole bone stiffness and stress distributions than isotropic models (Hazrati Marangalou et al., 2012; Kabel et al., 1999; Pahr and Zysset, 2009; Turner et al., 1990). The anisotropy of cancellous bone is largely determined by its microstructural organization. Theoretical and experimental studies demonstrated that the orthotropic principal directions and the anisotropic stiffness tensor can be well predicted from a second rank fabric tensor that describes the average orientation of this trabecular microarchitecture (Cowin, 1985; Cowin and Mehrabadi, 1989; Gross et al., 2013; Harrigan and Mann, 1984; Kabel et al., 1999; Odgaard et al., 1997; Zysset, 2003; Zysset et al., 1998). Measurement of such fabric tensors, however, requires images with a resolution that is good enough to resolve the trabecular architecture. For bone in-vivo, this presently is possible only for the peripheral skeleton (Boutroy et al., 2005; Burghardt et al., 2011; Burrows et al., 2010; Liu et al., 2010; MacNeil and Boyd, 2008). Although recent studies have introduced approaches to calculate such microstructural properties from clinical CT (Saha and Wehrli, 2004; Tabor et al., 2013; Tabor and Rokita, 2007) and high-resolution flat-panel CT systems (Bredella et al., 2008; Mulder et al., 2012), the accuracy of such measurements still has to be established.

In this study, we explore a different approach to derive patient-specific fabric information by using a database of high-resolution bone models. By combining the density information measured from a patient CT scan with fabric information from the database, patient-specific anisotropic properties can be defined. Presently, only a rather limited number ($n=33$) of bones are available for this database. The goal of this study therefore was to investigate if models with fabric derived from such a limited database can already produce more accurate results than isotropic models. To investigate this, we compared the stress and damage distribution as well as the whole bone stiffness and strength for FE models with fabric derived from the actual bone with those of model with fabric mapped from the database or isotropic mechanical properties.

## 2. Material and methods

### 2.1. Material

A database (DB) of 33 human cadaver femurs (mean age: 77.8 ± 10.0 year) obtained from 17 female and 16 male donors was generated for all these bones. Micro-CT scans (XtremeCT, Scanco Medical AG, Brüttisellen, Switzerland) of the most proximal part (9–12 cm in length) were made with a nominal isotropic resolution of 82 μm. Images were filtered and processed according to the protocol recommended by the manufacturer. Compartments of cortical and cancellous bone were identified using masks. A first mask comprising the whole bone was made based on the periosteal contour. In order to find the cortical shell, original images were filtered using a strong Gauss filter (sigma=5, support=5 voxels) and segmented using a threshold of 15% of the maximum gray-value, leaving only the cortical bone. This image was used to identify the cortical shell in the original mask. In addition, the most periosteal 1 mm region of the original mask was identified as part of the (sub)cortical compartment. The remainder of the mask was considered the cancellous compartment.

### 2.2. Creation of FE models

Continuum finite element models of the 33 proximal femurs were generated based on contours of the bone periosteal surface as obtained using software provided with the micro-CT scanner (IPL V5.16, Scanco Medical AG, Brüttisellen, Switzerland). Isotopological models were generated for each bone segment using a pre-defined mesh template based on a generalized femur geometry that contained approximately 300 thousand second order tetrahedron elements with a typical edge length of 2 mm. This mesh template was morphed onto the bone surface extracted from the micro-CT scan by identifying a minimum of 8 anatomical landmarks. After morphing, each element number identifies an element that, with good approximation, is at the same specific anatomical location in all samples (Grassi et al., 2011). Since the mesh template comprises the whole femur while the micro-CT scans only covered the most proximal part of these, the number of elements on the proximal femur models was less and varied from approximately 80,000–90,000 depending on the scan length.

To each element a volume fraction and morphological properties were assigned using a homogenization technique described earlier (Hazrati Marangalou et al., 2012). In summary: first, we determined whether the element was in the cortical or cancellous compartment. If an element was at the cortical/cancellous interface, we calculated what fraction of its volume was in each of both compartments. For each element that was at least partly within the cancellous bone, a spherical volume of interest around the element centroid with a diameter of 4 mm was defined (Harrigan et al., 1988). Trabecular bone architectural parameters, including bone volume fraction (BV/TV) and the mean intercept length (MIL)-based fabric tensor, were analyzed for the volume of interest as far as it was within the cancellous compartment using the image processing software provided by the micro-CT system. Measured morphological parameters were then assigned to the elements. For elements in the cortical compartment, only a volume fraction for the volume comprised by the element itself was defined whereas a rule of mixture was used for elements that cover both compartments based on the portion of the element volume within the cortical/cancellous compartments. Fig. 1 depicts mesh generation and bone morphology analysis procedures.

Ten femurs were randomly taken from the database as test cases. For each test case, three different FE models were generated. In the first model, orthotropic material properties were specified based on the actual fabric and density measurements of that bone. In the second FE model, orthotropic material properties were specified based on the actual density measurement and fabric derived from a corresponding DB model. To do so, the DB model with a density distribution most similar to that of the test bone was selected and its fabric was mapped to the test model. The test model itself was excluded from the database during the selection process. In the third FE model, isotropic material properties were specified based on the actual density measurements only (Fig. 2).

To select a DB model $j$ with a density distribution most similar to that of the test bone $i$, we selected the DB model that minimized the root-mean-square error

$$Err_i = min_{j=1}^{32}\left(\sqrt{\frac{\sum_{k=1}^{N_{elements}}(\rho_{i,k}-\rho_{j,k})^2}{N_{elements}}}\right) \quad (1)$$

with $N_{elements}$ the number of elements and $\rho_{i,k}$ the density of element $k$ of model $i$.

Whereas the use of the template enables an easy mapping and comparison of scalar properties between models, the mapping of tensor properties, such as fabric

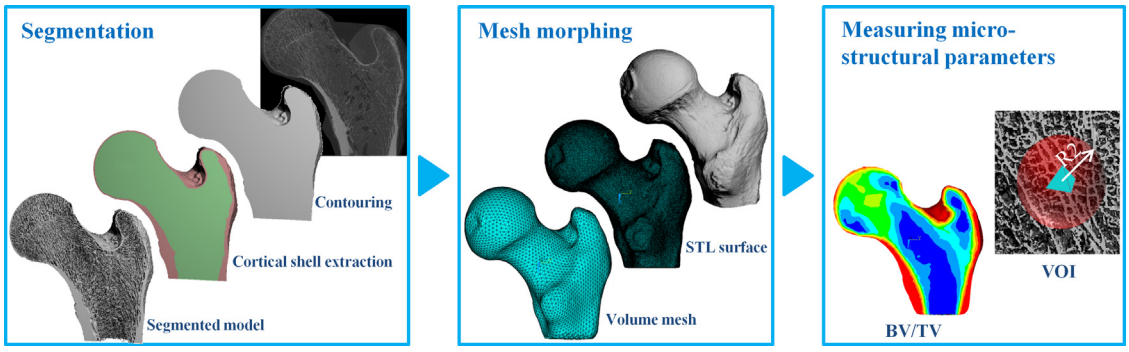


**Fig. 1.** FE models creation procedure for proximal femur models.

tensor is not straightforward. For these properties the principal directions must be also updated to account for differences in element orientation (Fig. 3a). The procedure proposed here to account for this is to define a local orthonormal coordinate system $\{\vec{e_1}, \vec{e_2}, \vec{e_3}\}$ for each element in the model. This coordinate system is based on the vectors $\vec{v_1}$ and $\vec{v_2}$ that are defined by the nodes of the tetrahedron element (Fig. 3b) using

$$\vec{e}_1 = \frac{\vec{v}_1}{|\vec{v}_1|}$$

$$\vec{e}_2 = \frac{(\vec{v}_1 \times \vec{v}_2) \times \vec{v}_1}{|(\vec{v}_1 \times \vec{v}_2) \times \vec{v}_1|}$$

$$\vec{e}_3 = \frac{\vec{v}_1 \times \vec{v}_2}{|\vec{v}_1 \times \vec{v}_2|} \tag{2}$$

For all elements a compliance tensor $\mathbb{C}$ was derived from the element density $\rho$ and fabric tensor $\mathbf{M}$ using the Zysset–Curnier relationship (Zysset and Curnier, 1995)

$$\mathbb{C} = \sum_{i=1}^{3} \frac{1}{\varepsilon_0 \rho^k m_i^{l2}} M_i \otimes M_i - \sum_{i,j=1; i \neq j}^{3} \frac{\nu_0}{\varepsilon_0 \rho^k m_i^l m_j^l} M_i \otimes M_j + \sum_{i,j=1; i \neq j}^{3} \frac{1}{2G_0 \rho^k m_i^l m_j^l} M_i \underline{\otimes} M_j \tag{3}$$

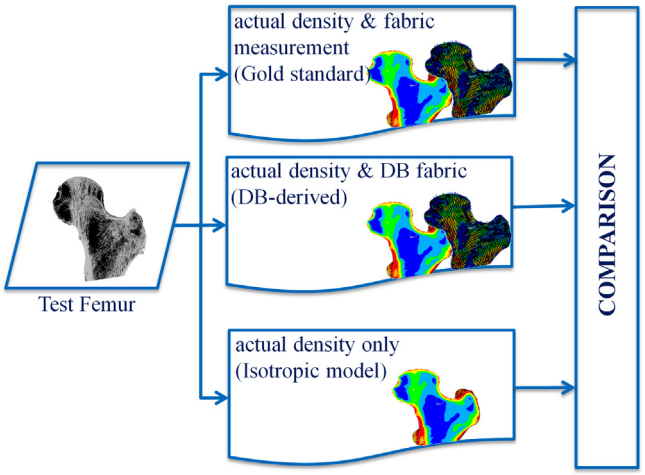


**Fig. 2.** Study design.

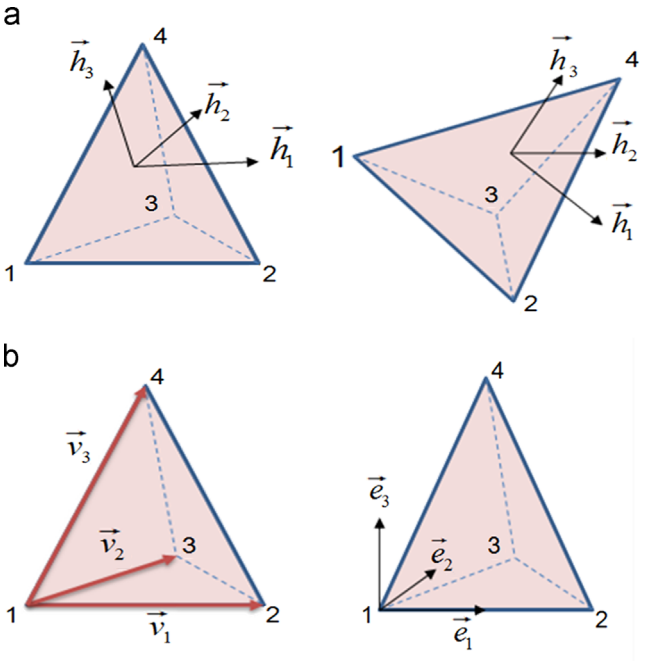


**Fig. 3.** (a) When the orientation of corresponding elements is not the same, the fabric principal directions must be rotated accordingly, (b) definition of the element local coordinate system based on vectors defined by its nodal points.

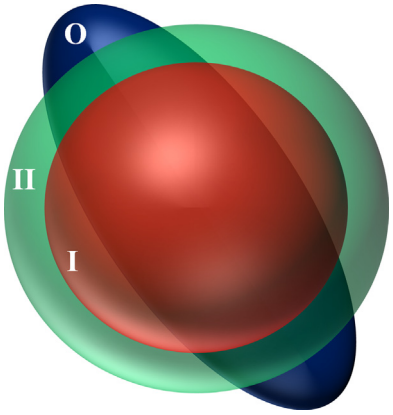


**Fig. 4.** Fabric tensor representation for orthotropic (O) and isotropic (I and II) models; models O and I were normalized such that det($\mathbf{M}$)=1, model II was scaled such that the total bone stiffness of models II and O is the same.

with $\varepsilon_0$, $\nu_0$ and $G_0$ elastic constants, $m_i$ the normalized eigen-values and $M_i$ the dyadic product of the eigenvectors of fabric tensor $\mathbf{M}$, det($\mathbf{M}$)=1.

For the isotropic models, the fabric tensor was replaced by a scaled identity tensor. Different choices, however, can be made for the scaling. In a first model (isotropic-I), the identity tensor was taken as the fabric tensor. As a consequence of this scaling the isotropic models will have a lower stiffness than the orthotropic model in the dominant principal direction (Fig. 4). For that reason, a second isotropic model was generated by scaling the fabric tensor ($\mathbf{M}=\alpha\mathbf{I}$, $\alpha>1$). The value of $\alpha$ was determined from a set of initial linear elastic analyses, in such a way that the stiffness of the scaled isotropic model is the same as that of the gold-standard model.

Elastic plastic damage constitutive behavior in the local form (Charlebois et al., 2010) was used to simulate failure and post-failure behavior of test femurs (Table 1). This material model contains a damage variable $D$ (ranging from $D=0$: no damage to $D=1$: fully damaged) to account for the reduction of stiffness due to propagation of voids and cracks, and due to breakage of individual trabeculae. Loading conditions applied to the models represented a fall to the side configuration (Courtney et al., 1995; Verhulp et al., 2008). The nodes on the surface of the greater trochanter, in a 3 mm layer were fixed in medio-lateral direction and the nodes at the distal end were fixed except for medio-lateral movements. The nodes at the femoral head medial side were fixed in all directions while a displacement in the lateral direction was applied to mimic a fall to the side condition. A total compressive displacement of 3 mm was applied in 100 load increments, and for each step the total reaction force was calculated. The force displacement curve maximum was taken as the femur ultimate load.

At the first load increment, the whole-bone stiffness was calculated from the reaction force and the applied displacement. At the last loading increment (3 mm displacement) the ultimate load was calculated from the reaction force. In addition, contour plots of the von Mises stress, the damage variable D and strain energy density were created.

Whole bone stiffness, ultimate load and the von Mises stress, damage and strain energy density distributions of the orthotropic models based on DB-derived fabric and the two isotropic models were compared to those of the orthotropic models based on actual fabric measurements, which were taken as the gold standard. Differences were quantified by calculating determination coefficients and relative root-mean-square errors (RRMSE)

$$RRMSE = \sqrt{\frac{\sum_{i=1}^{n}((x'_i - x_i)/x'_i)^2}{n}} \tag{4}$$

$x_i'$ are the values obtained from the gold standard models and $x_i$ are the values obtained from the isotropic or DB-derived models ($n=10$).

One-way ANOVA was used to test the significance of differences ($p<0.05$) between isotropic, DB-derived models and the gold standard in predictions of whole bone properties as well as damage/stress distributions.

## 3. Results

The major fabric value and its direction for a representative femur as obtained from direct measurement (left) and from the database mapping procedure (right) for a typical case are shown in Fig. 5. Overall, the fabric directions and values of the mapped model corresponded well with the measured one. Differences are most notable in the most distal end (due to an effect of the boundary) and in the region of Ward's triangle, which is due to the

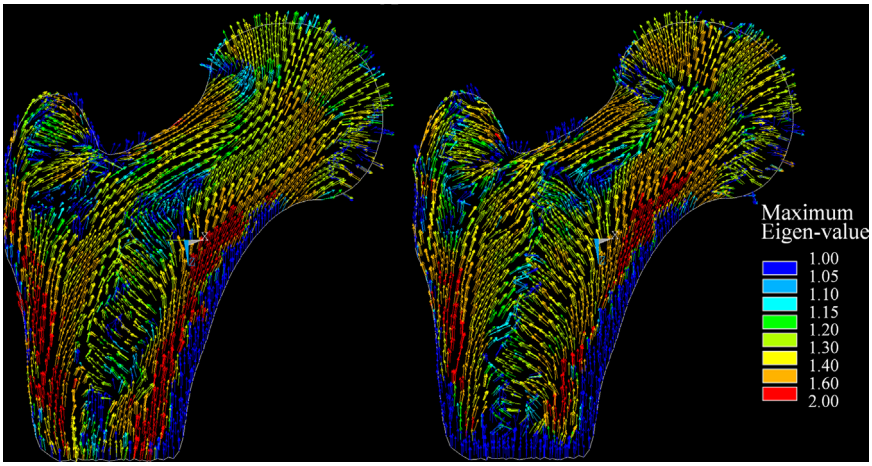


**Fig. 5.** Major fabric direction as obtained from the direct measurement (left) and from the database mapping procedure (right).

**Table 1**
Constants used in the material model (constants were taken from (Charlebois et al., 2010)).

| $E_0$ | $\nu_0$ | $k$ | $l$ | $\sigma^{0+}$ | $\sigma^{0-}$ | $\chi^{0+}$ | $\chi^{0-}$ | $p$ | $q$ | $\sigma^{H}$ | $s$ | $D_c$ | $a$ |
|---|---|---|---|---|---|---|---|---|---|---|---|---|---|
| 8237.1 | 0.18 | 2.5 | 1.88 | 57.4 | 132.4 | -0.748 | 0.340 | 2.5 | 0.86 | 6.0 | 37.5 | 0.6 | 22.5 |

low volume fraction in that region that makes the fabric measurement unreliable.

Contour plots of the von Mises stress (Fig. 6a) show that the isotropic model-I slightly underestimates the stresses, which is due to the fact that its stiffness in the anatomical directions is less. In contrast, the isotropic-II model overestimates the stresses. The DB-derived orthotropic model tends to slightly overestimate the stresses as well. In all cases, however, a good qualitative agreement with the gold-standard was obtained.

More pronounced differences were found when looking at the predicted damage distribution (Fig. 6b). The isotropic models underestimates the amount of damage in the neck regions, in particular for the isotropic-I model, whereas the DB-derived model well represents the distribution found for the gold-standard (Fig. 6b). Similar to the Damage and von Mises stress, DB-derived models slightly overestimated strain energy density (SED) values with respect to the gold standard in the femoral neck while the isotropic-I and isotropic-II models slightly underestimated SED values in particular near the femoral head (Fig. 6c).

Whole-bone force–displacement curves show that the DB-derived orthotropic model can accurately replicate the force–displacement curves found for the gold standard while the isotropic-I model underestimates both the stiffness and ultimate load (Fig. 7). The isotropic-II model with adjusted stiffness, on the other hand, clearly overestimates ultimate load (Fig. 7).

Compared to the gold standard, the relative root mean square error (RRMSE) for whole-bone stiffness was 4.9% for the DB-derived model and 26.3% for the isotropic-I model. For all ten femurs analyzed, the isotropic-I model underestimated whole bone stiffness. Nevertheless, the correlation between predicted and gold-standard values was very good, with a coefficient of determination $R^2=93.2\%$ for the isotropic-I model (Fig. 8). In this case also, a very good correlation was found for the DB-derived model with an $R^2=90.9\%$. We found a high one-to-one correlation for the DB-derived orthotropic model with the gold standard (CC=94.5%) while a low concordance correlation was found (CC=57.3%) for the isotropic-I models.

The isotropic-I models also underestimate the ultimate load with an RRMSE of 14.5% while the isotropic-II model overestimated the ultimate load with an RRMSE of 7.92%. For the DB-derived orthotropic model this error was 3.1%. In this case also, predicted and gold-standard values for the ultimate load correlated well for all cases, with a coefficient of determination $R^2=90.9\%$ for the isotropic-I model, $R^2=85.6\%$ for the isotropic-II model and $R^2=96.3\%$ for the DB-derived model (Fig. 8). Compared to the gold standard, there is a low concordance correlation between isotropic-I and the gold standard (CC=79.2%) and for the isotropic-II model (CC=88.9%) while this value for the DB-derived models is CC=97.6%.

One-way ANOVA revealed that there is a significant difference between isotropic-I models and the gold standard for whole bone stiffness ($p=0.039$) however no significant differences were found for failure load, neither for the isotropic-I model ($p=0.324$) nor for the isotropic-II model ($p=0.683$). Significant differences were found for the stress and damage distributions for both isotropic models and the gold standard. For the DB-derived models, neither the whole bone properties (stiffness/failure load) nor stress/damage distributions were significantly different from the gold standard.

## 4. Discussion

The goal of this study was to investigate if models with fabric derived from a limited database can produce more accurate results than isotropic models. We found that indeed this is the case. Whole bone properties (stiffness and failure load) and stress and damage distributions were better predicted by the DB-derived orthotropic model than by the isotropic model. In fact, no significant differences were found for all these properties, whereas significant differences were found for the isotropic models tested here for whole bone stiffness, stress distribution and damage distribution.

As different approaches exist to make an isotropic model from an existing anisotropic one, we tested two different approaches. With the first one, the fabric tensor was made isotropic and normalized such that its determinant remained the same as in the orthotropic case, with the other approach the fabric tensor was scaled such that the whole bone stiffness would be the same as that of the orthotropic model. Other choices would have been possible as well. For example, in many studies isotropic models are

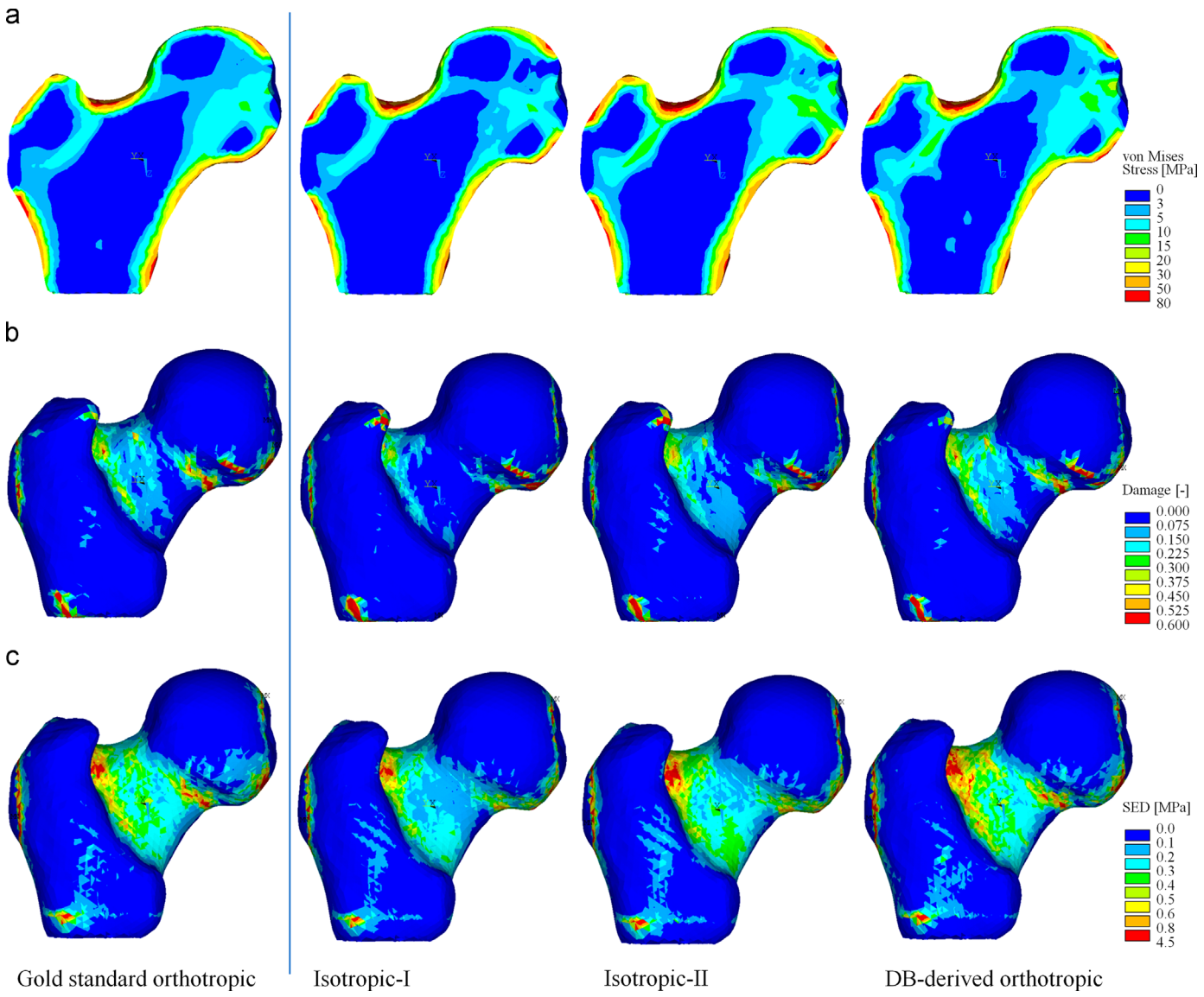


**Fig. 6.** (a) von Mises stress, (b) damage parameter and (c) strain energy density (SED) distribution in the gold standard, isotropic-I, isotropic-II and DB-derived orthotropic models respectively from left to the right.

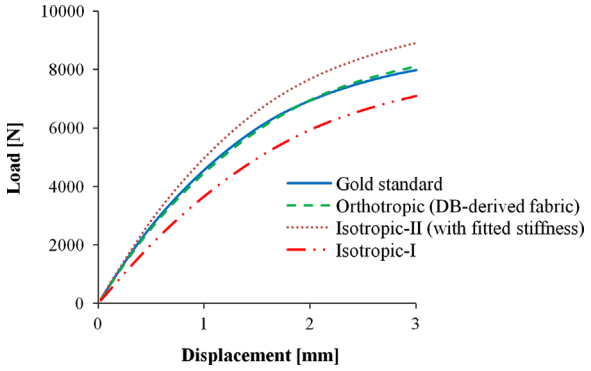


**Fig. 7.** Typical force–displacement curves obtained from different orthotropic and isotropic models for a femur model under fall to the side condition.

used with material properties based on laws that relate the stiffness in the anatomical direction to the bone density (such as the Carter and Hayes (1977) and Ashman et al. (1989) relationships). In such studies, the highest modulus is assigned in all directions. In our study, this would correspond to scaling the fabric tensor such that its value equals the largest value of the orthotropic model. Clearly, this would result in an overprediction of bone stiffness and ultimate load. Since the isotropic-II models used in our study here already led to an overprediction of stresses and strength, we did not further consider this option.

In our study we used fall-to-the-side boundary conditions because we expected that effects of anisotropy for this non-habitual loading case would be more pronounced than for physiological loading conditions. During physiological loading conditions, the bone will be loaded in its principal fabric direction. In that situation, the use of experimentally-derived relationships that relate the stiffness in the anatomical direction to the bone density might produce more accurate results than in our study. Nevertheless, this load case is commonly used for analyses of bone strength. Also, implants will lead to non-habitual loading conditions of bone, atleast locally. We thus think the results here are relevant for many situations.

In this study, we did not explicitly investigate the sensitivity of the database approach for errors in the mesh morphing and mapping procedure, however this error was addressed implicitly. Since the mesh morphing tool was used 33 times to generate the

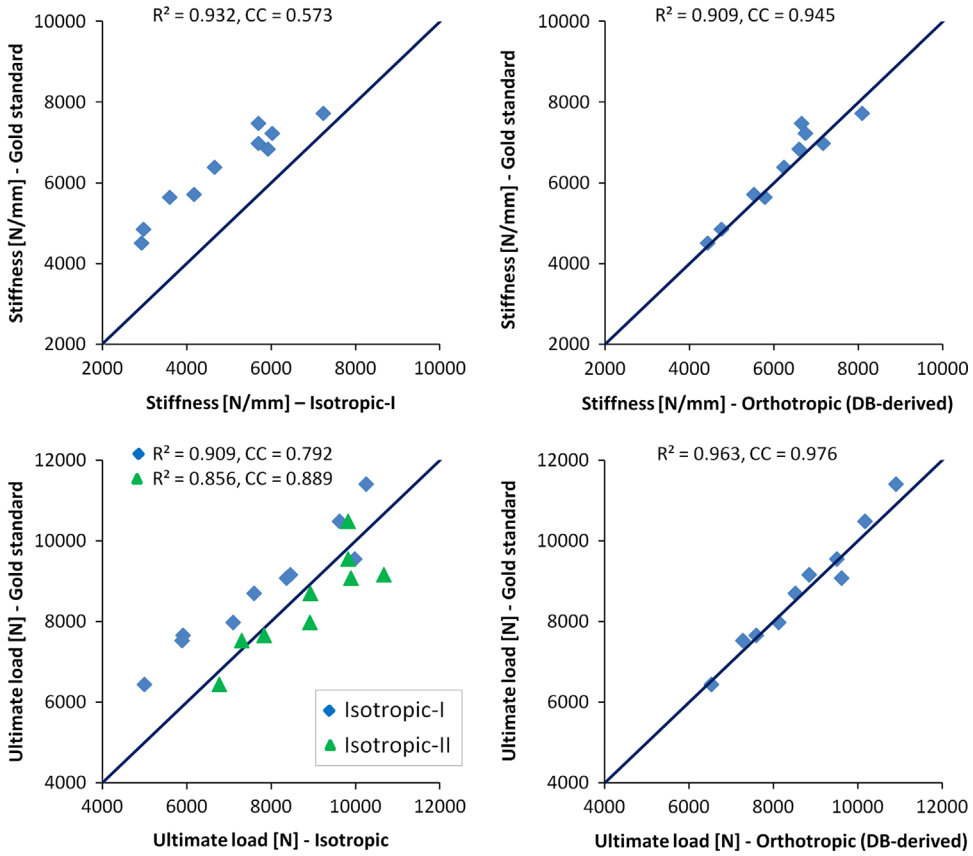


**Fig. 8.** Correlation of isotropic and DB-derived orthotropic models with the gold standard in whole bone stiffness (upper row) and ultimate load (bottom row) predictions; (solid line: 45° line, CC: concordance correlation).

femur database in this study, large deviations from the intended anatomical position would lead to larger RRMS errors in density distribution. However the results show that for the ten test cases used in this study, good correlations were found. On average the correlation between the density of a test bone and its selected DB entry was $R=91\%$ (89–92%) while on average the RMSE was 0.11 (0.10–0.12), demonstrating that in all cases a bone was found in the DB that has a very similar density distribution. In clinical practice, however, the patient image would be obtained from a clinical CT scanner rather than from the same micro-CT scanner as in our study. It is possible that this will lead to a less favorable fit. Nevertheless, since reliable density information can be obtained from clinical CT scanners as well, we expect that in that case also the same database model would be selected.

Some limitations of this study must be mentioned as well. First the database generated in this study contained only 33 femurs. Although this was large enough to improve results in this study, it might not cover enough cases needed when used for larger populations. Increasing the number of database entries, however, is trivial and would increase the accuracy in database selection procedure and would result in more accurate prediction of bone orthotropic material properties.

Second, we use only one parameter (BV/TV) in our selection model to choose the model which best matches the patient model. In particular, we did not consider the size or shape of the bone. Adding more parameters such as shape parameters (e.g. femoral neck angle or other anthropometric parameters or results from modal analyses (Cheng et al., 1997; Taylor et al., 2002) or other parameters such as age in addition to the density distribution might result in more accurate results. In this study, however adding more selection criteria is not feasible due to the limited number of database entries.

Third, mesh quality is a crucial factor in the fabric mapping procedure. Since a local element-based coordinate system is used to map the fabric tensor from the best matching database model to patient model, severe deformities of elements (e.g. tetrahedrons with high aspect ratios) would introduce inaccuracies in the procedure. We found that in some regions the fabric orientation can be inaccurate due to element distortion. However, apparently such errors do not much affect the whole bone and stress distribution results.

Fourth, the mesh template geometry did not distinguish explicitly between the cancellous and cortical compartments, such that elements can be in both compartments. To make sure that a clear cortical region exists, we assumed a minimum thickness of 1 mm for the cortical region, although previous studies have shown that the cortical shell thickness can be less than 1 mm at some locations (Treece et al., 2010; Yan et al., 2003). We do not expect this assumption will affect our results much though, since, with our approach a cortical thickness of less than 1 mm would also result in a lower density of the cortical element and thus would be accounted for. Furthermore, we only quantified morphological parameters in the cancellous bone region, not for the cortical region. The determination of cortical morphological parameters, such as cortical thickness and cortical porosity from micro-CT scans is possible as well. However, cortical thickness cannot be assigned per element since at most locations the thickness is larger than the element size, whereas cortical porosity is similar to the density that is calculated for the cortical elements. A more accurate representation of the cortical and cancellous compartments would require separate templates for cortical and cancellous bone. Since this would considerably complicate the meshing and mapping procedure, we decided to cover both compartments with one mesh template.

Finally, we used a local formulation of the constitutive law of Charlebois et al. whereas non-local formulations are available as well. However, since a typical length scale for cancellous bone would be round 1 mm, and since our elements also are about the same in size, we expect that a local and non-local formulation would provide very similar results.

In conclusion, the approach presented here can be used to create patient-specific anisotropic finite element models of bones even in cases where the bone fabric cannot be measured in-vivo. The mesh-morphing approach used here can be used as a versatile tool to map the missing fabric information, as well as any other micro-structural information to the patient models. We expect that this approach can lead to more accurate results in particular in cases where bone anisotropy plays an important role, such as in osteoporotic patients and around implants.

## Conflict of interest statement

Bert van Rietbergen is a consultant for Scanco Medical AG.

## Acknowledgments

Funding from the European Union for the Osteoporotic Virtual Physiological Human Project (VPHOP FP7-ICT2008-223865) is gratefully acknowledged.

## References

Ashman, R.B., Rho, J.Y., Turner, C.H., 1989. Anatomical variation of orthotropic elastic moduli of the proximal human tibia. Journal of Biomechanics 22, 895–900.

Boutroy, S., Bouxsein, M.L., Munoz, F., Delmas, P.D., 2005. In Vivo assessment of trabecular bone microarchitecture by high-resolution peripheral quantitative computed tomography. Journal of Clinical Endocrinology and Metabolism 90, 6508–6515.

Bredella, M.A., Misra, M., Miller, K.K., Madisch, I., Sarwar, A., Cheung, A., Klibanski, A., Gupta, R., 2008. Distal radius in adolescent girls with anorexia nervosa: trabecular structure analysis with high-resolution flat-panel volume CT1. Radiology 249, 938–946.

Burghardt, A., Link, T., Majumdar, S., 2011. High-resolution computed tomography for clinical imaging of bone microarchitecture. Clinical Orthopaedics and Related Research 469, 2179–2193.

Burrows, M., Liu, D., McKay, H., 2010. High-resolution peripheral QCT imaging of bone micro-structure in adolescents. Osteoporosis International 21, 515–520.

Carter, D., Hayes, W., 1977. The compressive behavior of bone as a two-phase porous structure. Journal of Bone and Joint Surgery, American volume 59, 954–962.

Charlebois, M., Jirasek, M., Zysset, P.K., 2010. A nonlocal constitutive model for trabecular bone softening in compression. Biomechanics and Modeling in Mechanobiology 9, 597–611.

Cheng, X.G., Lowet, G., Boonen, S., Nicholson, P.H.F., Brys, P., Nijs, J., Dequeker, J., 1997. Assessment of the strength of proximal femur in vitro: relationship to femoral bone mineral density and femoral geometry. Bone 20, 213–218.

Courtney, A.C., Wachtel, E.F., Myers, E.R., Hayes, W.C., 1995. Age-related reductions in the strength of the femur tested in a fall-loading configuration. Journal of Bone and Joint Surgery, American volume 77, 387–395.

Cowin, S.C., 1985. The relationship between the elasticity tensor and the fabric tensor. Mechanics of Materials 4, 137–147.

Cowin, S.C., Mehrabadi, M.M., 1989. Identification of the elastic symmetry of bone and other materials. Journal of Biomechanics 22, 503–515.

Grassi, L., Hraiech, N., Schileo, E., Ansaloni, M., Rochette, M., Viceconti, M., 2011. Evaluation of the generality and accuracy of a new mesh morphing procedure for the human femur. Medical Engineering & Physics 33, 112–120.

Gross, T., Pahr, D., Zysset, P., 2013. Morphology–elasticity relationships using decreasing fabric information of human trabecular bone from three major anatomical locations. Biomechanics and Modeling in Mechanobiology 12, 793–800.

Harrigan, T.P., Jasty, M., Mann, R.W., Harris, W.H., 1988. Limitations of the continuum assumption in cancellous bone. Journal of Biomechanics 21, 269–275.

Harrigan, T.P., Mann, R.W., 1984. Characterization of microstructural anisotropy in orthotropic materials using a second rank tensor. Journal of Materials Science 19, 761–767.

Hazrati Marangalou, J., Ito, K., van Rietbergen, B., 2012. A new approach to determine the accuracy of morphology–elasticity relationships in continuum FE analyses of human proximal femur. Journal of Biomechanics 45, 2884–2892.

Helgason, B., Perilli, E., Schileo, E., Taddei, F., Brynjólfsson, S., Viceconti, M., 2008. Mathematical relationships between bone density and mechanical properties: a literature review. Clinical Biomechanics 23, 135–146.

Kabel, J., van Rietbergen, B., Odgaard, A., Huiskes, R., 1999. Constitutive relationships of fabric, density, and elastic properties in cancellous bone architecture. Bone 25, 481–486.

Keller, T.S., 1994. Predicting the compressive mechanical behavior of bone. Journal of Biomechanics 27, 1159–1168.

Keyak, J.H., 2001. Improved prediction of proximal femoral fracture load using nonlinear finite element models. Medical Engineering and Physics 23, 165–173.

Liebschner, M.A.K., Kopperdahl, D.L., Rosenberg, W.S., Keaveny, T.M., 2003. Finite element modeling of the human thoracolumbar spine. Spine 28, 559–565.

Liu, X.S., Zhang, X.H., Sekhon, K.K., Adams, M.F., McMahon, D.J., Bilezikian, J.P., Shane, E., Guo, X.E., 2010. High-resolution peripheral quantitative computed tomography can assess microstructural and mechanical properties of human distal tibial bone. Journal of Bone and Mineral Research 25, 746–756.

Lotz, J.C., Gerhart, T.N., Hayes, W.C., 1991. Mechanical properties of metaphyseal bone in the proximal femur. Journal of Biomechanics 24, 317–329.

MacNeil, J.A., Boyd, S.K., 2008. Bone strength at the distal radius can be estimated from high-resolution peripheral quantitative computed tomography and the finite element method. Bone 42, 1203–1213.

Mulder, L., van Rietbergen, B., Noordhoek, N.J., Ito, K., 2012. Determination of vertebral and femoral trabecular morphology and stiffness using a flat-panel C-arm-based CT approach. Bone 50, 200–208.

Odgaard, A., Kabel, J., van Rietbergen, B., Dalstra, M., Huiskes, R., 1997. Fabric and elastic principal directions of cancellous bone are closely related. Journal of Biomechanics 30, 487–495.

Pahr, D.H., Zysset, P.K., 2009. A comparison of enhanced continuum FE with micro FE models of human vertebral bodies. Journal of Biomechanics 42, 455–462.

Saha, P.K., Wehrli, F.W., 2004. A robust method for measuring trabecular bone orientation anisotropy at in vivo resolution using tensor scale. Pattern Recognition 37, 1935–1944.

Tabor, Z., Petryniak, R., Latała, Z., Konopka, T., 2013. The potential of multi-slice computed tomography based quantification of the structural anisotropy of vertebral trabecular bone. Medical Engineering and Physics 35, 7–15.

Tabor, Z., Rokita, E., 2007. Quantifying anisotropy of trabecular bone from gray-level images. Bone 40, 966–972.

Taddei, F., Schileo, E., Helgason, B., Cristofolini, L., Viceconti, M., 2007. The material mapping strategy influences the accuracy of CT-based finite element models of bones: an evaluation against experimental measurements. Medical Engineering and Physics 29, 973–979.

Taylor, W.R., Roland, E., Ploeg, H., Hertig, D., Klabunde, R., Warner, M.D., Hobatho, M.C., Rakotomanana, L., Clift, S.E., 2002. Determination of orthotropic bone elastic constants using FEA and modal analysis. Journal of Biomechanics 35, 767–773.

Treece, G.M., Gee, A.H., Mayhew, P.M., Poole, K.E.S., 2010. High resolution cortical bone thickness measurement from clinical CT data. Medical Image Analysis 14, 276–290.

Turner, C.H., Cowin, S.C., Rho, J.Y., Ashman, R.B., Rice, J.C., 1990. The fabric dependence of the orthotropic elastic constants of cancellous bone. Journal of Biomechanics 23, 549–561.

Verhulp, E., van Rietbergen, B., Huiskes, R., 2008. Load distribution in the healthy and osteoporotic human proximal femur during a fall to the side. Bone 42, 30–35.

Wirtz, D.C., Schiffers, N., Pandorf, T., Radermacher, K., Weichert, D., Forst, R., 2000. Critical evaluation of known bone material properties to realize anisotropic FE-simulation of the proximal femur. Journal of Biomechanics 33, 1325–1330.

Yan, K., Engelke, K., Kalender, W.A., 2003. A new accurate and precise 3-D segmentation method for skeletal structures in volumetric CT data. IEEE Transactions on Medical Imaging 22, 586–598.

Yosibash, Z., Padan, R., Joskowicz, L., Milgrom, C., 2007. A CT-based high-order finite element analysis of the human proximal femur compared to in-vitro experiments. Journal of Biomechanical Engineering 129, 297–309.

Zannoni, C., Mantovani, R., Viceconti, M., 1999. Material properties assignment to finite element models of bone structures: a new method. Medical Engineering and Physics 20, 735–740.

Zysset, P.K., 2003. A review of morphology–elasticity relationships in human trabecular bone: theories and experiments. Journal of Biomechanics 36, 1469–1485.

Zysset, P.K., Curnier, A., 1995. An alternative model for anisotropic elasticity based on fabric tensors. Mechanics of Materials 21, 243–250.

Zysset, P.K., Goulet, R.W., Hollister, S.J., 1998. A global relationship between trabecular bone morphology and homogenized elastic properties. Journal of Biomechanical Engineering 120, 640–646.